Astronomy & Astrophysics manuscript no. nPDF_paperII
March 4, 2025
©ESO 2025

arXiv:2503.01160v1 [astro-ph.GA] 3 Mar 2025

Turbulence in virtual

II. Origin of skewness and dual fraction processes

Xunchuan Liu (刘训川)[1,2]

[1] Leiden Observatory, Leiden University, P.O. Box 9513, 2300RA Leiden, The Netherlands
e-mail: liuxunchuan001@gmail.com
[2] Shanghai Astronomical Observatory, Chinese Academy of Sciences, 80 Nandan Road, Shanghai 200030, PR China

Draft Feb 2025

ABSTRACT

Turbulence is a mysterious phenomenon in physical systems and plays a critical role in the interstellar medium (ISM). Previous simulations and observations have shown that the probability density functions (PDFs) of gas densities in supersonic systems tend to be skewed, exhibiting low-density exponential tails on the $s = \ln\rho$ scale. In this work, we argue that these exponential tails originate from the convolution of PDF kernels with skewed tails, which can appear at both ends of the PDF. Skewness has limited influence on the $\sigma^2 - \mathcal{M}$ relation. We introduce two density-fraction strategies – the mass-fraction and volume-fraction approaches – to explain the physical origins of the low-s and high-s skewed PDF kernels. These two types of PDF kernels define two spaces of skewed PDFs, which are dual to each other and possess highly symmetric mathematical structures. We thus speculate that the high-s skewed PDF kernels are physical and may be related to the power-law tails of the column-density PDFs (on the ρ scale) of molecular clouds, which are shaped by both turbulence and gravity. Inspired by this, we further construct a form of an 'isothermal' turbulent system that likely favors the volume-fraction strategy.

Key words. Turbulence — ISM: kinematics and dynamics — ISM: clouds

1. Introduction

Turbulence is a fundamental aspect of fluid dynamics (Kolmogorov 1941; Burgers 1948) and plays a key role in astrophysical and interstellar environments. Together with gravity and possibly magnetic fields, it shapes the evolution of gas in molecular clouds (e.g., Orkisz et al. 2017), star-forming regions (e.g., Liu et al. 2025b), and other astrophysical systems (e.g., Veltri 1999; Read et al. 2020; Paneque-Carreño et al. 2024), influencing the transport of energy, momentum, and mass (e.g., Larson 1981; McKee & Tan 2003). Despite its significance, the origin of interstellar turbulence remains uncertain. It is thought to arise from large-scale ISM dynamics, with contributions from various driving mechanisms, including shear motions (e.g., Miyamoto et al. 2014), stellar feedback (e.g., Carroll et al. 2009; Gent 2012), cloud-cloud interactions (e.g., Wu et al. 2018), and gravitational instabilities (e.g., Goldbaum et al. 2015).

A key feature of turbulent systems of compressible gas is the probability density function (PDF) of density, which has been found to follow a log-normal distribution in simulations (Vazquez-Semadeni 1994; Padoan et al. 1997; Federrath et al. 2010). However, simulations also show that for supersonic systems (with Mach number $\mathcal{M} > 1$), especially those driven by compressive forcing, the PDFs are log-normal at the high-density end but tend to skew toward the low-density (and low $s = \ln(\rho)$) end (e.g., Federrath et al. 2010). In observations, due to the projection effect, only column density is accessible, which follows a log-normal distribution in gravity-non-dominated regions (Berkhuijsen & Fletcher 2008; Schneider et al. 2015; Liu et al. 2025a). Such a low-s skewed log-normal PDF has also been observed in the HI 21 cm line emission of a very high-velocity cloud, observed with the FAST 500-m telescope (Liu et al. 2025a).

The physical origin of the skewness in the PDFs of turbulent systems (referred to as the skewness of turbulence) remains an open question. Hopkins (2013), interpreting turbulence as a cascading process that broadens the PDF through convolution at successive cascade levels (Kolmogorov 1941; Castaing 1996; Yakhot 1998), speculated that the low-s skewness arises from PDF convolution kernels due to intermittency. However, they did not explicitly demonstrate how intermittency generates exponential tails from physical principles. Beyond the lack of a physical explanation for turbulence skewness, there is also a more intrinsic motivation for this study. In Paper I of this series, we provided a thermodynamic perspective of the relationship between PDF variance (σ^2) and $\mathcal{M}$. It is therefore natural for us to continue to investigate the origin of PDF skewness and its impact on the σ^2–$\mathcal{M}$ relation.

In this work, we mathematically explore how exponential tails lead to skewed PDFs at both the low-s and high-s ends and provide a direct physical explanation for the skewed PDF kernels. Precise mathematical forms of the PDF kernels are derived. The work is structured as follows: In Section 2, we present background information on PDFs and PDF kernels with exponential tails. In Section 3, we describe two density-fraction strategies to explain the origins of the PDF kernels skewed at both ends. In Section 4, we introduce the 'dual' concept of PDFs and explore the high symmetry between the PDF kernels resulting from the two different strategies. Section 5 presents further discussion. Specifically, in Section 5, we prove that the PDF kernels derived are consistent with the requirements of the $\Sigma^2 - \mathcal{M}$ relation from Paper I; in Section 5.2, we discuss why and how the high-s

skewed kernels are physical by preliminarily exploring the mathematical construction of corresponding turbulent systems.

2. PDF skewness

2.1. Basic definitions

A normalized PDF (on the logarithmic scale $s = \ln(\rho)$) should satisfy the following conditions (see also Paper I):

$$\int f_\tau(s)\, ds = 1, \tag{1}$$

$$\int f_\tau(s) e^s\, ds = 1. \tag{2}$$

Let g and h be two normalized PDFs, and let $f * g$ denote their convolution. It can be shown that:

$$\begin{aligned}\int (g * h)(s) e^s\, ds &= \int g(s-t) h(t) e^s\, dt\, ds \\ &= \int h(t) e^t\, dt = 1.\end{aligned} \tag{3}$$

Thus, $g * h$ is also a normalized PDF. Let $\sigma^2(g)$ denote the variance of g. Then, the variance of $g * h$ satisfies

$$\sigma^2(g * h) = \sigma^2(g) + \sigma^2(h). \tag{4}$$

If we further assume that $g \propto e^{ax}$ and $h \propto e^{bx}$ for $x < 0$, with $a > b > 0$, then:

$$g * h \propto \int e^{ay} e^{b(x-y)}\, dy \propto e^{bx} \quad \text{for } x \to -\infty. \tag{5}$$

Therefore, convolution cannot introduce the exponential tail of the convolution kernels. The resulting convolved curve will have an exponential index equal to that of the convolution kernel with the flattest tail.

2.2. PDF kernels

2.2.1. PDF kernels of low-s skewness by H13

Hopkins (2013), having noticed the special role of the exponential PDF kernels described above, successfully fitted the low-s-skewed PDF. One of the key ideas of the H13 model is to construct the PDF by repeatedly convolving a low-s-end skewed kernel on the logarithmic scale. The form of the kernel they chosen is

$$f_\tau(s) = A \exp\left(-\frac{s_{\rm cut} - s}{\tau}\right) (s < s_{\rm cut}). \tag{6}$$

To make f_τ normalized,

$$s_{\rm cut} = \ln(1+\tau), \tag{7}$$

$$A = \frac{1}{\tau}. \tag{8}$$

A PDF with the exponential tail of f_τ and a dispersion σ_0 can be constructed through repeatedly convolved f_τ by λ times with (Hopkins 2013):

$$\lambda = \frac{\sigma_0^2}{\tau^2}. \tag{9}$$

The resultant PDF, $f_{\tau;\lambda}$, is (Hopkins 2013):

$$\begin{aligned} f_{\tau;\lambda}(s) &= (f_\tau)^{*\lambda}(s) \\ &= \frac{1}{\Gamma(\lambda)} \frac{1}{\tau} \left(\frac{\lambda \ln(1+\tau) - s}{\tau}\right)^{\lambda-1} \exp\left(-\frac{|s - \lambda\ln(1+\tau)|}{\tau}\right). \end{aligned} \tag{10}$$

with $f_{\tau;n}(s) = 0$ for $s > \lambda \ln(1+\tau)$. Here, $f^{*\lambda}$ denotes the successive convolution of λ instances of f. To implement this convolution process with non-integer λ, Hopkins (2013) treated it as a variable following a Poisson distribution with a mean of σ_0^2/τ^2.

2.2.2. PDF kernel of high-s skewness

In Eq. 6, $f_\tau(s)$ is presumed to skew to the low-s end. However, under physical effects such as gravity, it may skew to the high-s end. Similarly, we can define a high-s-skewed f_τ^+ as:

$$f_\tau^+(s) = A^+ \exp\left(-\frac{s - s_{\rm cut}^+}{\tau}\right) \quad (s > s_{\rm cut}^+), \tag{11}$$

where,

$$s_{\rm cut}^+ = \ln(1-\tau), \tag{12}$$

$$A^+ = \frac{1}{\tau}. \tag{13}$$

Unlike the low-s-skewed case, here, τ must be smaller than 1 to ensure mass conservation. $f_{\tau;n}^+$ can be constructed in the same manner as $f_{\tau;n}$ (Sect. 2.2.1).

f_τ and f_τ^+ are not just symmetric in mathematical form. In the following sections, we will provide a physical explanation of f_τ and f_τ^+, along with their modified forms, demonstrating that they are actually linked to two kinds of fraction strategies. Moreover, the high-s-skewed PDF kernel may not be as unphysical as it initially appears.

3. Two fraction strategies

Similar to the velocity cascading process in turbulence, the density of compressive gas in a turbulent system is also expected to develop in a cascading and self-similar manner. Below, we propose two strategies for the density fraction process of a single step in detail and present the explicit forms of their corresponding PDF kernels (on the logarithmic scale).

3.1. Mass fraction and low-s-skew PDF

Here, we consider two buckets of equal unit volume, each containing a unit mass (upper panel of Fig. 1). In a single mass exchange process, the buckets randomly exchange a mass δm, where δm follows a uniform distribution between -1 and 1. This is why we refer to it as the mass-fraction strategy. It can be shown that the distribution of the mass within one bucket (or the density) follows $f_{\tau=1}$.

Now, we consider that in each step, there are vritually N independent repetitions of such mass exchange processes. Based on the principle of least action, the mass exchange process that minimizes the mass difference (i.e., the one with the smallest $|\delta m|$) is the one actually executed in that step. Note that the total mass is conserved. As a result, one of the two buckets will have a density smaller than 1, while the other will have a density greater than 1. For the bucket with the lower density, the probability that its density is less than ρ (where $\rho < 1$) is given by

$$\mathrm{CDF}_{N,Mf}(\rho) = \frac{1}{2}\rho^N. \tag{14}$$

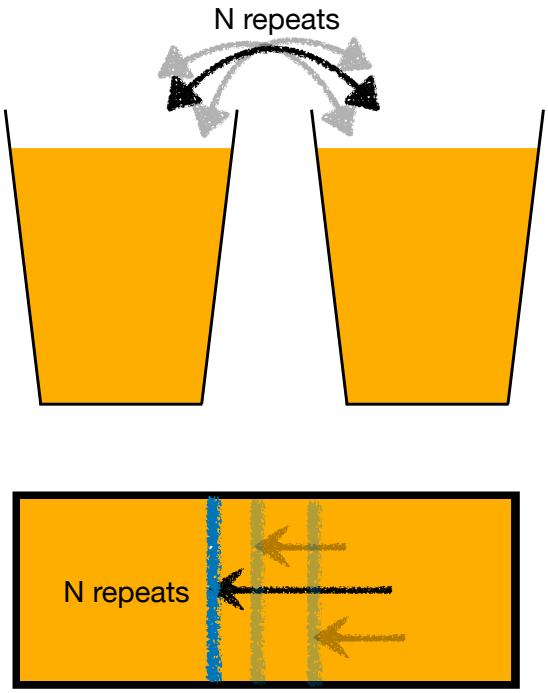

Fig. 1. Sketch map of density fraction strategies: Mass fraction (top) and volume fraction (bottom) strategies (Sect. 3). Among the N virtual realizations of the processes, the one that creates the smallest difference between the two subvolumes is realized.

Thus, the PDFs of ρ and s for that bucket are

$$P_{N,Mf}(\rho) = \frac{d\,\mathrm{CDF}_{N,Mf}}{d\rho} = \frac{N}{2}\rho^{N-1}, \tag{15}$$

$$P_{N,Mf}(s) = P_{N,Mf}(\rho)\frac{d\rho}{ds} = \frac{N}{2}\rho^{N} = \frac{N}{2}e^{Ns}. \tag{16}$$

Comparison between Eqs. 16 and 6 yields $\tau = 1/N$. For the bucket with $\rho > 1$, due to mass conservation, the PDFs are given by

$$P_{N,Mf}(\rho) = P_{N,Mf}(2-\rho) = \frac{N}{2}(2-\rho)^{N-1}, \tag{17}$$

$$P_{N,Mf}(s) = \frac{N}{2}(2-e^{s})^{N-1}e^{s}. \tag{18}$$

We thus suggest a modified form of f_τ:

$$f_{\tau;\mathrm{modif}} = \begin{cases} \dfrac{1}{2\tau}e^{s/\tau} & \text{for } s \le 0, \\ \dfrac{1}{2\tau}\left(2-e^{s}\right)^{\frac{1-\tau}{\tau}}e^{s} & \text{for } 0 < s < \ln(2). \end{cases} \tag{19}$$

The procedure outlined above ensures that $f_{\tau;\ \mathrm{modif}}$ is a normalized PDF, satisfying Eqs. 1 and 2.

The upper panel of Fig. 2 shows a comparison between f_τ and $f_{\tau;\ \mathrm{modif}}$. For small τ (or equivalently small N), $f_{\tau;\ \mathrm{modif}}$ tends to be more symmetric, implying that $f_{\tau;\ \mathrm{modif}}$ may be more physically realistic than f_τ. However, a small τ typically corresponds to the case of low $\mathcal{M}$, where the PDF kernels are repeatedly convolved multiple times, ultimately approaching a Gaussian-like PDF. In this scenario, there is little difference between the different convolution kernels. In Fig. 3, we compare $(f_{\tau;\mathrm{modif}})^{*n}$ and $f_{\tau;\lambda}$ (Sect. 2.2.1) with the same τ and σ^2. They are similar to each other, especially at the low-s end where skewness occurs. Note

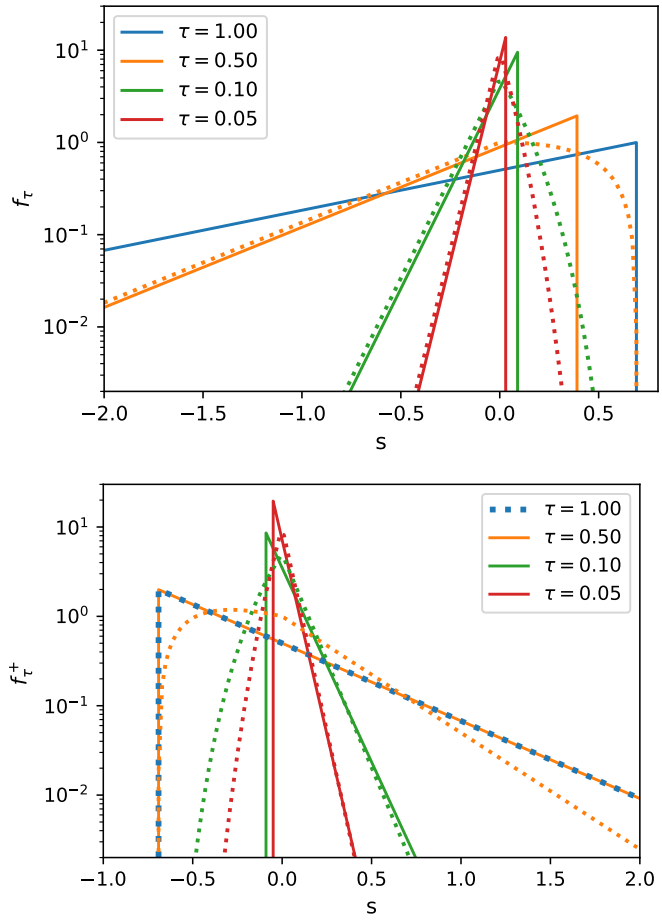

Fig. 2. Upper: The black solid lines show f_τ for different values of τ (Eq. 6). Dotted lines represent $f_{\tau;\mathrm{modif}}$, the modification of f_τ suggested by Eq. 19. Lower: Same as the upper panel but for f^+_τ (solid) and $f^+_{\tau;\mathrm{modif}}$ (dotted) (see Eqs. 11 and 31). Note that for $\tau = 1$, f^+_τ is undefined.

that for small τ, the variance $\sigma^2(f_{\tau;\ \mathrm{modif}})$ is no longer τ^2, as is the case for f_τ. Instead, we have (Fig. 4)

$$\sigma^2(f_{\tau;\ \mathrm{modif}}) \sim 2\tau^2, \quad \text{as } \tau \to 0. \tag{20}$$

A drawback of the modified kernel is that to construct a PDF with a variance of σ^2 through convolution from $f_{\tau;\ \mathrm{modif}}$, the repetitions of the kernels cannot simply be given by σ^2/τ^2.

For the super-extreme case of $f_{\tau;\mathrm{modif}}$ with $\tau \to \infty$, $N = 1/\tau \to 0$, although N cannot be an integer, the equations from Eq. 14 to Eq. 19 remain valid mathematically. Let $\tau \to \infty$, we have

$$f_{\tau\to\infty;\ \mathrm{modif}} = \begin{cases} \sim \dfrac{1}{2\tau} & \text{for } -\tau < s \le 0, \\ \sim \dfrac{1}{2\tau}\dfrac{e^{s}}{2-e^{s}} & \text{for } 0 < s \le \ln(2-e^{-\tau}). \end{cases} \tag{21}$$

There is another form of the above equation:

$$f_{\tau\to\infty;\ \mathrm{modif}} \sim \begin{cases} \dfrac{1}{2\tau} & \text{for } -\tau < s < \ln(2-e^{-\tau}), \quad (22) \\ \dfrac{1}{2}\,\mathrm{Dirac}(\ln(2)) & \text{for } s = \ln(2). \quad (23) \end{cases}$$

Here, Dirac represents the Dirac delta function. Note that the mass integral ($\int e^{s} f\, ds$) of Eq. 22 converges to 0 as $\tau \to \infty$, while the integral of Eq. 23 is 1. In this context,

$$f_{\tau\to\infty;\ \mathrm{modif}} \sim \mathrm{Dirac}(\ln(2)). \tag{24}$$

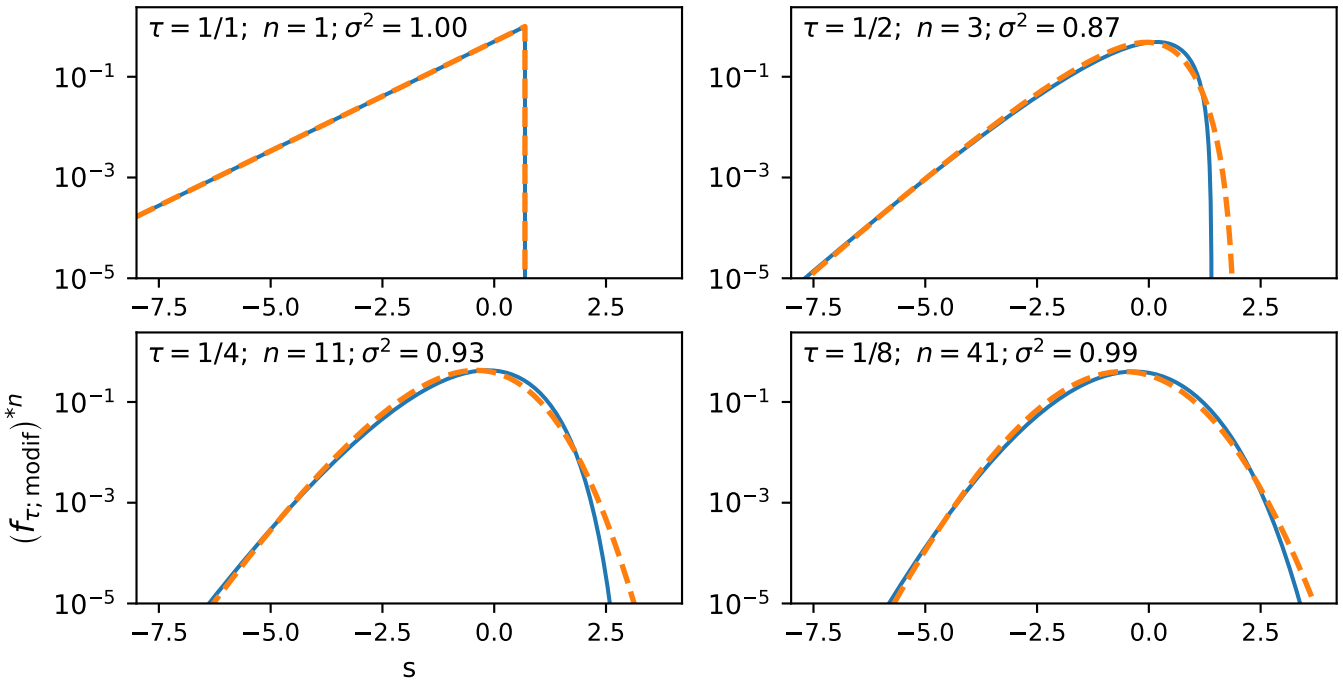

Fig. 3. In each panel, the yellow dashed line represents $(f_{\tau;\mathrm{modif}})^{*n}$, the result of the successive convolution of n instances of $(f_{\tau;\mathrm{modif}})$. The parameters τ and n, as well as the σ^2 of $(f_{\tau;\mathrm{modif}})^{*n}$, are labeled in the upper left corner. The blue solid line corresponds to $f_{\tau,\lambda}$ with a τ identical to that of $f_{\tau;\mathrm{modif}}$, and $\lambda = \sigma^2/\tau^2$, ensuring that $(f_{\tau;\mathrm{modif}})^{*n}$ and $f_{\tau,\lambda}$ have the same σ^2. Note that for $\tau = 1$ and $n = 1$, the two curves overlap because, in this case, there is no modification (Sect. 3.1).

3.2. Volume fraction and high-s-skew PDF

The mass-fraction strategy described above maintains the volumes of the buckets while exchanging the mass they contain. This motivates the consideration of another strategy in which the mass is not exchanged, but the volumes of the buckets are altered. We refer to this strategy as the volume-fraction strategy (Fig. 1).

In the volume-fraction strategy, we consider a slab that divides a large volume ($\mathcal{V}_{\mathrm{tot}} = 2$) into two buckets, each containing a mass of 2 (Fig. 1). In a single volume exchange process, the slab is randomly moved, resulting in a volume difference ($\delta\mathcal{V}$) between the two buckets, which follows a uniform distribution between -1 and 1. Similar to the mass-fraction strategy, we now consider that in each step, there are virtually N independent repetitions of such volume exchange processes, and the volume exchange process that minimizes the volume difference is the one actually executed in that step. Then, for the bucket with $s > 0$ (or equivalently $\mathcal{V} < 1$), we have

$$\mathrm{CDF}_{N,Vf}(\mathcal{V}) = \frac{1}{2}\mathcal{V}^N, \tag{25}$$

$$P_{N,Vf}(\mathcal{V}) = \frac{N}{2}\frac{1}{\mathcal{V}^{N+1}}, \tag{26}$$

$$P_{N,Vf}(s) = \frac{N}{2}e^{-Ns}. \tag{27}$$

Again, a comparison between Eqs. 27 and 11 leads to $\tau = 1/N$. For the bucket with $\rho < 1$, due to volume conservation, the PDF can be written as

$$P_{N,Vf}(s) = \frac{N}{2}(2 - e^{-s})^{N-1}e^{-s}. \tag{28}$$

It seems to suggest that the modified form of f^+_τ is

$$f^+_{\tau;\ \mathrm{modif};\ \dagger} = \begin{cases} \dfrac{1}{2\tau}e^{-s/\tau} & \text{for} \quad s \geq 0, \\ \dfrac{1}{2\tau}\left(2 - e^{-s}\right)^{\frac{1-\tau}{\tau}} e^{-s} & \text{for} \quad \ln\left(\dfrac{1}{2}\right) < s < 0. \end{cases} \tag{29}$$

with good symmetry with $f_{\tau;\mathrm{modif}}(-s)$:

$$f^+_{\tau;\ \mathrm{modif};\ \dagger}(s) \equiv f_{\tau;\mathrm{modif}}(-s). \tag{30}$$

However, $f^+_{\tau;\ \mathrm{modif};\ \dagger}$ is not a normalized PDF; it satisfies Eq. 1 but not Eq. 2. The key point is that the PDF discussed in this work is a volume-weighted statistic. In the volume fraction strategy, a weight proportional to $\mathcal{V} = 1/\rho = e^{-s}$ must be taken into account. Thus, we adopt a modified form of f^+_τ (Fig. 2):

$$f^+_{\tau;\ \mathrm{modif}}(s) = e^{-s}f^+_{\tau;\ \mathrm{modif};\ \dagger} = e^{-s}f_{\tau;\ \mathrm{modif}}(-s). \tag{31}$$

It can be verified that $f^+_{\tau;\ \mathrm{modif}}$ satisfies both Eqs. 1 and 2. This is not a coincidence; for further discussion, see Sect. 4. The simple mathematical form of Eq. 31 suggests that the two density-fraction strategies are, in some sense, symmetric to each other.

As in Eqs. 22 and 23, we have

$$f^+_{\tau\to\infty;\ \mathrm{modif}} \sim \begin{cases} \dfrac{e^{-s}}{2\tau} & \text{for } \ln(e^{-\tau} - 2) < s < \tau, \quad (32) \\ \mathit{Dirac}(-\ln(2)) & \text{for } s = -\ln(2). \quad (33) \end{cases}$$

Unlike in Eq. 24, here we cannot omit Eq. 32, because its mass integral is non-zero:

$$\int_0^\tau \frac{e^{-s}}{2\tau}e^s\,ds = \frac{1}{2}. \tag{34}$$

Thus, half of the mass of the system will contribute to the high-s exponential tail of Eq. 32.

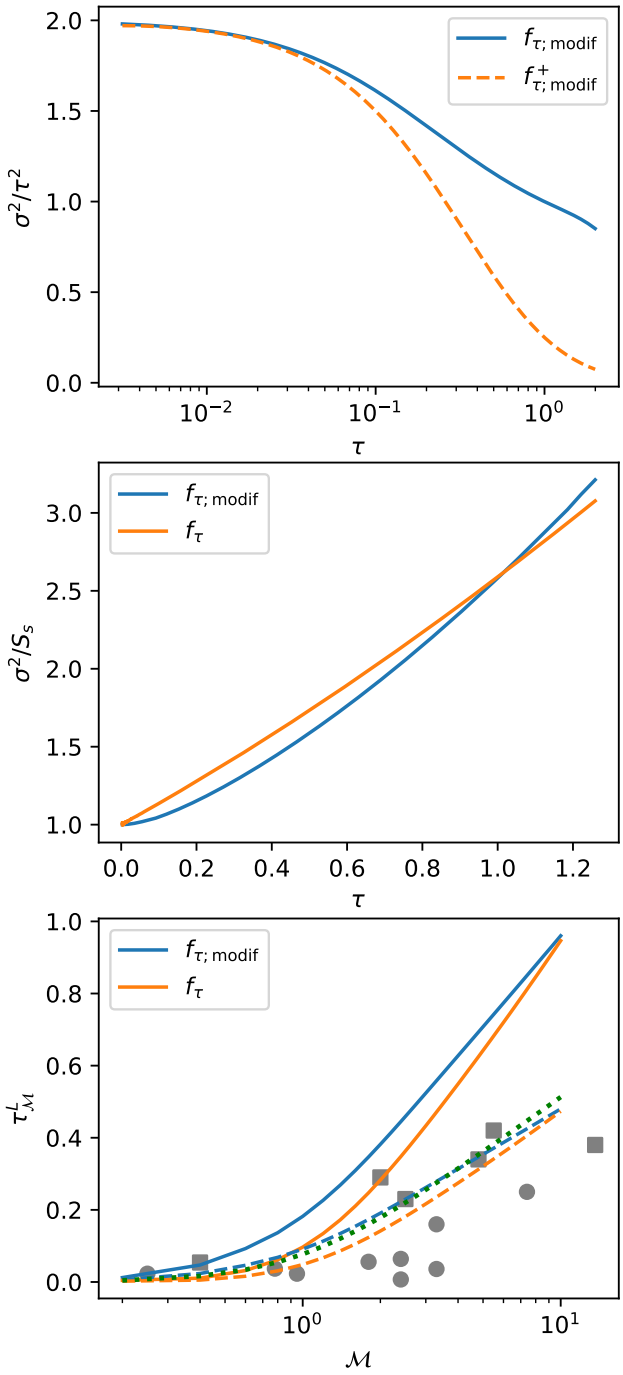

Fig. 4. Upper: The ratio of the variance of the kernels to τ^2, for $f_{\tau;\mathrm{modif}}$ (blue) and $f^{+}_{\tau;\mathrm{modif}}$ (orange). Middle: The ratio between the variance (σ^2) and the structural entropy (S_s) of the kernels. Lower: The solid lines show the curves of $\tau^L_{\mathcal{M}}$ (see Sect. 5.1 for details). The dashed lines are the solid lines divided by a factor of 2. The green dotted line is $\ln(1+\mathcal{M}^2)/9$. The gray squares and circles show the τ of $f_{\tau;\lambda}$ fitted by Hopkins (2013), based on simulations driven by compressive and solenoidal forcing, respectively.

4. Duality between the two fraction strategies

In this section, we demonstrate that the low-s-skew PDFs and high-s-skew PDFs are 'dual' to each other. This confirms, from a mathematical standpoint, the speculation that the two density-fraction strategies (Sect. 3) are fundamental and orthogonal strategies, and thus may both occur in turbulent systems, under specific conditions.

Let $f(s)$ be any normalized PDF that satisfies both Eqs. 1 and 2, and denote the dual of f as

$$f^{\mathrm{dual}}(s) \equiv \mathrm{Dual}[f](s) = e^{-s} f(-s). \tag{35}$$

Then, we have:

$$\int f^{\mathrm{dual}}(s)\,ds = \int e^{-s} f(-s)\,ds = \int e^{s} f(s)\,ds = 1, \tag{36}$$

$$\int e^{s} f^{\mathrm{dual}}(s)\,ds = \int f(-s)\,ds = \int f(s)\,ds = 1. \tag{37}$$

So, P^{dual} is also a normalized PDF, and

$$\mathrm{Dual}[f^{\mathrm{dual}}](s) \equiv f(s). \tag{38}$$

From the above equations, it can be easily proved that $f^{+}_{\tau;\,\mathrm{modif}}$ (Eq. 30) is a normalized PDF, since $f^{+}_{\tau;\,\mathrm{modif}} = \mathrm{Dual}[f_{\tau;\,\mathrm{modif}}]$.

We define a space of purely low-s-skewed PDFs, denoted $\mathcal{F}_L$, as follows:

1. For any $\tau > 0$, $f_{\tau,\,\mathrm{modif}} \in \mathcal{F}_L$;
2. For any integer $n > 1$ and $f_{\tau_i} \in \mathcal{F}_L$ for $i = 1, \ldots, n$, the convolution $f_{\tau_1} * f_{\tau_2} * \cdots * f_{\tau_n} \in \mathcal{F}_L$.
3. For any f and g in $\mathcal{F}_L$ and $0 \le t \le 1$, $tf + (1-tg) \in \mathcal{F}_L$.

Any $f \in \mathcal{F}_L$ has an exponential tail (as $s \to -\infty$) with an exponential factor of $1/\min(\tau_i)$. Similarly, we can define a space of purely high-s-skewed PDFs, denoted $\mathcal{F}_H$ from $f^{+}_{\tau;\,\mathrm{modif}}$.

Note that the operations of dual and convolution are exchangeable:

$$\begin{aligned} f^{\mathrm{dual}}(s) * g^{\mathrm{dual}}(s) &= [f(-s)e^{-s}] * [g(-s)e^{-s}] \\ &= [f(-s) * g(-s)] \cdot e^{-s} \\ &= f * g(-s) \cdot e^{-s} \\ &= (f * g)^{\mathrm{dual}}(s), \end{aligned} \tag{39}$$

Also, we have

$$af^{\mathrm{dual}} + bg^{\mathrm{dual}} = (af + bg)^{\mathrm{dual}}. \tag{40}$$

It follows that

$$\mathrm{Dual}[f] \in \mathcal{F}_H \qquad \text{for } f \in \mathcal{F}_L, \tag{41}$$

$$\mathrm{Dual}[f] \in \mathcal{F}_L \qquad \text{for } f \in \mathcal{F}_H. \tag{42}$$

$\mathcal{F}_L$ and $\mathcal{F}_H$ are dual to each other:

$$Dual[\mathcal{F}_L] = \mathcal{F}_H, \quad Dual[\mathcal{F}_H] = \mathcal{F}_L. \tag{43}$$

Similarly, we define a space $\mathcal{F}$ of skewed PDFs generated from $f_{\tau;\,\mathrm{modif}}$ and $f^{+}_{\tau;\,\mathrm{modif}}$. We have

$$Dual[\mathcal{F}] = \mathcal{F}. \tag{44}$$

Any $f \in \mathcal{F}$ can be uniquely decomposed as the convolution of two PDFs: one in $\mathcal{F}_L$ and one in $\mathcal{F}_H$. Pure Gaussian PDFs, denoted as P, can be viewed as a special case of skewed PDFs and approximated by Gaussian-like functions $f \in \mathcal{F}$. Note that,

$$\mathrm{Dual}[P] = P. \tag{45}$$

5. Discussion

5.1. Influence of skewness on $\sigma^2 - \mathcal{M}$ relation

In Paper I, it is shown that for a Gaussian-like PDF (f) on the logarithmic scale, the structural entropy is

$$S_s(f) = -2\int f s e^s\, ds = -\sigma^2(f), \tag{46}$$

where σ^2 is the variance of f. Now, we check whether the skewed PDF kernels of f_τ and $f_{\tau,\,\mathrm{modif}}$ also obey such a relation.

For f_τ, $\sigma^2(f_\tau) = \tau^2$. When τ is small (see the middle panel of Fig. 4),

$$S_s(f_\tau) \sim \tau^2 = \sigma^2 \quad \text{as } \tau \to 0. \tag{47}$$

However, the ratio of σ^2/S_s grows as τ increases.

For $f_{\tau,\,\mathrm{modif}}$ with $N = 1/\tau \gg 1$, the value of S_s is[1]

$$\begin{aligned} S_s(f_{\tau;\mathrm{modif}}) &= -\int_0^1 N\rho^N \ln(\rho)\, d\rho - \int_1^2 N(2-\rho)^{N-1}\rho\ln(\rho)\, d\rho \\ &= \frac{N}{(N+1)^2} - \int_0^1 N\rho^{N-1}(2-\rho)\ln(2-\rho)\, d\rho \\ &\sim \tau\left(\frac{1}{1+2\tau} - \left(\frac{2}{1+\tau} - \frac{1}{1+3\tau}\right)(1-\tau)\right) \\ &\sim -2\tau^2 \sim -\sigma^2(f_{\tau;\mathrm{modif}}). \end{aligned} \tag{48}$$

However, the ratio of σ^2/S_s also increases with τ. The σ^2/S_s for f_τ and $f_{\tau,\,\mathrm{modif}}$ are similar to each other (Fig. 4).

In Paper I, we propose a delay parameter q to explain the deviation of the PDF variance from the empirical $\sigma^2 - \mathcal{M}$ relation for turbulent systems driven by compressive forcing. Here, we denote the deviation factor as $X(\mathcal{M})$, and $\mathcal{M}$ should be interpreted as the Mach number of the compressive velocity component ($\mathcal{M}_{\mathrm{comp}}$; see Paper I). If such a deviation is fully due to the skewness of the kernel (f_τ or $f_{\tau;\,\mathrm{modif}}$), then we should get a lower limit of τ as

$$\tau^L_{\mathcal{M}} = \mathrm{solve}\left(\frac{\sigma^2(f_\tau)}{S_s(f_\tau)} = X(\mathcal{M}),\ \tau\right). \tag{49}$$

Here, $\tau^L_{\mathcal{M}}$ is the lower limit because the PDF would approach a lognormal distribution after convolution, and thus the ratio $\frac{\sigma^2}{S_s}$ will approach 1. The curve of $\tau^L_{\mathcal{M}}$ along $\mathcal{M}$ is shown in the bottom panel of Fig. 4, for both f_τ and $f_{\tau;\,\mathrm{modif}}$. The τ values, obtained by fitting the simulated PDFs using $f_{\tau,\lambda}$ as done by Hopkins (2013), are also shown. The fitted τ values are all smaller than $\tau^L_{\mathcal{M}}$. We thus conclude that the PDF skewness cannot fully explain the deviation of the $\sigma^2 - \mathcal{M}$ relation.

An auxiliary result can be obtained from the dashed and dotted lines in the bottom panel of Fig. 4. For turbulent systems with compressive forcing, the following equation may serve as a rough estimation of the $\tau - \mathcal{M}$ relation:

$$\tau_{\mathcal{M}} = 0.5\tau^L_{\mathcal{M}} \sim \frac{1}{\mathcal{D}^2}\ln(1+\mathcal{M}^2), \tag{50}$$

with $\mathcal{D} = 3$ the dimension of the system. We do not know if such a relation still holds for 2D systems. For turbulent systems driven by solenoidal forcing, $\tau_{\mathcal{M}}$ is even lower (Fig. 4). We thus suggest that PDF skewness (τ) and variance are two relevant, but not fully dependent, statistical parameters of turbulent systems.

[1] Note that $\int_1^2 x^N \ln(x)dx = \frac{{}_2F_1(1,2+N,3+N,1/2)}{2(1+N)(2+N)}$.

5.2. High-s-skewness systems

The low-s and high-s skewed PDF kernels, derived from two different density fraction strategies, are dual to each other with a highly symmetric mathematical structure. Thus, it is very likely that the high-s-skewed PDF kernel is physical. Molecular clouds, which can be treated as isothermal systems governed by both turbulence and gravity, usually show high-density-end power-law tails (on the ρ scale; corresponding to exponential tails on the s scale) on their PDFs of column densities (e.g., Schneider et al. 2013; Brunt 2015; Alves et al. 2017; Zhang et al. 2025). Simulations also confirm this phenomenon (e.g., Veltchev et al. 2024). We speculate that it may be related to the high-s-skewed PDF kernels promoted in this work. Initiated by this idea, we try to construct turbulent systems that biases toward high-s skewed PDFs.

The Mach number plays a critical role in turbulence, so the isothermal feature should be at least partly maintained. The momentum equation of isothermal gas fluid is

$$\frac{\partial \mathbf{v}}{\partial t} + (\mathbf{v}\cdot\nabla)\mathbf{v} = -\frac{1}{\rho}\nabla P - \Delta\phi, \tag{51}$$

with

$$P = \rho c_s^2 = \rho T_{\mathrm{thermal}}. \tag{52}$$

Here, c_s is the sound speed, and $c_s^2 = T_{\mathrm{thermal}}$ ignoring constant terms. In a turbulence-gravity coupling system, a gravity-bound region that is suddenly compressed by turbulence will typically provide positive pressure due to its density-enhanced boundary. However, as the density structure adjusts under the influence of gravity, that region may provide weak or even no pressure to counteract the external pressure. Thus, analogously, we construct a system that does not contain the $\Delta\phi$ term, and instead has a modified pressure term:

$$P = \rho T\,\mathcal{L}(\mathcal{D}, det(\mathcal{H})). \tag{53}$$

Here, $\mathcal{L}$ is a function of $\mathcal{D} = \nabla(\rho\mathbf{v})$ and $\mathcal{H}$ is the Hessian matrix of ρ. The simplest form of $\mathcal{L}$ is

$$\mathcal{L}(x,y) = \begin{cases} 1-\Omega & \text{for } x>0, y<0, \\ 1 & \text{otherwise.} \end{cases} \tag{54}$$

That is, when the gas is locally compressed, the pressure term works normally (Eq. 52). When the density-enhanced region is expanding, the pressure term is reduced. If $\Omega = 0$, the system reverts to the normal state. If $\Omega = 1$, a velocity convergent region will increase its density and never return to its previous state. This is the essence of the volume-fraction strategy. We thus speculate that, within this framework, Ω describes the weight of the volume-fraction strategy. Under the influence of gravity, the molecular cloud (in regions above a certain threshold) behaves similarly, leading to high-s skewed PDFs, provided the density-enhanced region has not yet globally collapsed under gravity. A detailed investigation of the system's behavior (Eq. 54) and its connection to the skewness of PDFs will be left for future exploration.

6. Summary

In this work, we explore the PDF kernels of turbulence skewness at both the low-s and high-s ends and attempt to associate them with direct physical explanations. We argue that these exponential tails originate from the convolution of PDF kernels with skewed tails, which can appear at both ends of the PDF. The main results include

1. We found that the PDF kernels with low-s skewed exponential tails can be explained by the virtual density fraction through a so-called mass-fraction strategy. Similarly, the high-s skewed kernels can be explained by a so-called volume-fraction strategy.
2. The explicit forms of the PDF kernels are derived. The two types of PDF kernels, produced by different strategies, exhibit highly symmetric structures. We introduce the concept of 'duality' to describe the relationship between the spaces of high-s-skewed and low-s-skewed PDFs.
3. Skewness has limited influence on the $\sigma^2 - \mathcal{M}$ relation. We suggest that PDF skewness (τ) and variance are two relevant, but not fully dependent, statistical parameters of turbulent systems.
4. We speculate that the high-density power-law tails of the column density PDFs of molecular clouds may be related to the high-s-skewed PDF kernels. Inspired by this, we briefly describe a form of turbulent system that may prefer the volume-fraction strategy.

Overall, we believe that the duality between the low-s and high-s skewed PDF kernels explored here may reveal intrinsic relations between different density-fraction strategies. Identifying such relations in the future may enhance our understanding of turbulence, particularly in isothermal and compressible systems.

Acknowledgements. X. Liu acknowledges the support of the Strategic Priority Research Program of the Chinese Academy of Sciences under Grant No. XDB0800303, and the National Key R&D Program of China under Grant No. 2022YFA1603100. X. Liu also thanks the Leiden University for providing working space of this work.

References

Alves, J., Lombardi, M., & Lada, C. J. 2017, A&A, 606, L2
Berkhuijsen, E. M. & Fletcher, A. 2008, MNRAS, 390, L19
Brunt, C. M. 2015, MNRAS, 449, 4465
Burgers, J. M. 1948, in Advances in Applied Mechanics, ed. R. V. Mises & T. V. Kármán, Vol. 1 (Elsevier), 171–199
Carroll, J. J., Frank, A., Blackman, E. G., Cunningham, A. J., & Quillen, A. C. 2009, ApJ, 695, 1376
Castaing, B. 1996, Journal de Physique II, 6, 105
Federrath, C., Roman-Duval, J., Klessen, R. S., Schmidt, W., & Mac Low, M. M. 2010, A&A, 512, A81
Gent, F. A. 2012, PhD thesis, Newcastle University Upon Tyne, UK
Goldbaum, N. J., Krumholz, M. R., & Forbes, J. C. 2015, ApJ, 814, 131
Hopkins, P. F. 2013, MNRAS, 430, 1880
Kolmogorov, A. 1941, Akademiia Nauk SSSR Doklady, 30, 301
Larson, R. B. 1981, Monthly Notices of the Royal Astronomical Society, 194, 809
Liu, X., Liu, T., Li, P.-S., et al. 2025a, arXiv e-prints, arXiv:2502.10897
Liu, X., Liu, T., Mai, X., et al. 2025b, arXiv e-prints, arXiv:2501.17502
McKee, C. F. & Tan, J. C. 2003, ApJ, 585, 850
Miyamoto, Y., Nakai, N., & Kuno, N. 2014, PASJ, 66, 36
Orkisz, J. H., Pety, J., Gerin, M., et al. 2017, A&A, 599, A99
Padoan, P., Nordlund, A., & Jones, B. J. T. 1997, MNRAS, 288, 145
Paneque-Carreño, T., Izquierdo, A. F., Teague, R., et al. 2024, A&A, 684, A174
Read, P. L., Young, R. M. B., & Kennedy, D. 2020, Geoscience Letters, 7, 10
Schneider, N., André, P., Könyves, V., et al. 2013, ApJ, 766, L17
Schneider, N., Ossenkopf, V., Csengeri, T., et al. 2015, A&A, 575, A79
Vazquez-Semadeni, E. 1994, ApJ, 423, 681
Veltchev, T. V., Girichidis, P., Marinkova, L., et al. 2024, MNRAS, 528, 432
Veltri, P. 1999, Plasma Physics and Controlled Fusion, 41, A787
Wu, B., Tan, J. C., Nakamura, F., Christie, D., & Li, Q. 2018, PASJ, 70, S57
Yakhot, V. 1998, Phys. Rev. E, 57, 1737
Zhang, C., Liu, T., Jiao, S., et al. 2025, arXiv e-prints, arXiv:2501.16682